




## Research Article

# COMSOL Simulation for Design of Induction Heating System in VULCAN Facility

Jinkun Min <sup>1,2</sup>, Guangyu Zhu <sup>2,3,4</sup>, Yidan Yuan,<sup>2</sup> and Jingquan Liu <sup>1</sup>

<sup>1</sup>Tsinghua University, Beijing 100084, China

<sup>2</sup>China Nuclear Power Engineering Co., Ltd, Beijing 100840, China

<sup>3</sup>Nuclear and Radiation Safety Center, MEE, Beijing 100082, China

<sup>4</sup>State Environmental Protection Key Laboratory of Nuclear and Radiation Safety Regulatory Simulation and Validation, Beijing 102488, China

Correspondence should be addressed to Jingquan Liu; [jingquan@tsinghua.edu.cn](mailto:jingquan@tsinghua.edu.cn)

Received 4 March 2021; Accepted 11 August 2021; Published 20 August 2021

Academic Editor: Leon Cizelj

Copyright © 2021 Jinkun Min et al. This is an open access article distributed under the Creative Commons Attribution License, which permits unrestricted use, distribution, and reproduction in any medium, provided the original work is properly cited.

The experimental facility VULCAN was setup to study the fuel-coolant interaction (FCI) phenomena in a postulated severe accident of light water reactors. The heating system is important for the facility to prepare molten material in a crucible. This article is concerned with the design of the heating system, which applies electromagnetic induction heating method. The COMSOL code was employed to simulate the induction heating characteristics of a graphite crucible under different current and frequency of the work coil (inductor). Given a frequency, the relationship between the crucible's average temperature and the inductor's current is obtained, which is instrumental to select the power supply of the induction heating system. Meanwhile, the skin effect of induction heating is analyzed to guide the choice of frequency and inductor of the heating system. According to the simulation results, the induction heating system of frequency 47 kHz is suitable for the experiment, with a good agreement in temperature between the measured and the predicted.

## 1. Introduction

During a hypothetical severe accident in light water reactors (LWR), molten fuel (corium) may get contact with coolant (water), resulting in fuel-coolant interactions (FCI). Under certain conditions, the heat transfer area between the melt and coolant will increase rapidly, and the time scale of heat transfer becomes much smaller than the time scale of decompression, which may lead to the generation of shock wave. This violent phase-change phenomenon is called steam explosion [1]. During a severe accident of a nuclear power plant, the steam explosion may cause a strong shock wave that affects the availability of equipment in the containment and even destroy the integrity of the pressure vessel and containment [2]. The steam explosions were extensively investigated by many research projects, including the OECD/NEA projects SERENA Phase I and Phase II launched in 2002 and 2008, respectively [3, 4], and both experiment and simulation

were directed to reduce the uncertainty caused by material properties and experimental conditions for steam explosions. Yet, steam explosion is still an unresolved issue for severe accident research, as indicated by the high-level ranking of research priorities in severe accident concluded from the EU project SARNET (Severe Accident Research NETwork of Excellence) in 2014 [5].

Experiments related to FCI can be divided into two categories, decoupled and coupled experiments, in terms of physical phenomena. The decoupled experiments are separate-effect tests performed to address the physical phenomena involved in FCI, such as the breakup of a melt jet and collapse of the vapor film. Vapor film collapse experiments usually use solid balls or heating tubes instead of melt to study the criteria of vapor film collapse [6, 7]. The vapor film behavior under different experimental conditions was also widely studied, including the difference of the vapor film behavior between a moving ball and a stationary ball [8, 9], the influence of shock wave on vapor

film [10], and the influence of different solutions on vapor film [11–14]. The experiments of jet breakup are usually performed in an isothermal system to study the influence of hydrodynamics on the behavior of jet in FCI [15–17]. More attention was paid to the influence of experimental conditions, such as jet material and coolant material on jet breakup [18, 19]. Coupled experiments were the integral tests performed to investigate the multiple physical mechanisms of FCI, in large scale of 10~1000 kg [20–25] and medium/small scale of 1 g~10 kg [26–30] of melt mass. Large-scale experiments are intended to obtain the general picture of FCI process, while small- and medium-scale experiments are focused on the understanding of physical mechanisms in FCI.

The present study is concerned with the development of a small-scale test facility, named the VULCAN (Violent interaction of molten fUeL with CoolANt) facility, which is conceived to perform fundamental experiment of high-temperature single droplet falling into a water pool under well-controlled conditions, with the objective to investigate the physical mechanisms of fuel-coolant interactions. In particular, the focus is the design of the heating system employed in the VULCAN facility.

The preparation and release of the molten droplet are important to the success of such a very high-temperature experiment. The heating methods are different in the previous studies according to the characteristics of the melt materials employed in experiment. The electrode heating method of the FARO experiment [20–23] is characterized by long service life and simple operation. It requires electrical conduction of melt material to create an arc between the electrodes. The KROTOS experiment [24] heats the experimental material by radiation of tungsten element that heated by resistive heating. This method has no additional requirement for material, but the radiation heat transfer makes the heating rate slow. The TRIO experiment [25] adopted a cold crucible with direct induction heating of melt material in a solidified shell of the melt itself. The method greatly reduces the requirements of crucible material, and it is applicable to prototypical material of corium. However, the cold crucible has complexity in operation and difficulty in energy balance between induction power and heat dissipation, which may cause instability of the cold crucible wall. The DEFOR [28, 29] and MISTEE [30] experiments adopt the induction heating of a crucible, which heats the melt material, i.e., so-called “hot-crucible” method, which is simple to operate and easy to implement.

Given the small scale of the VULCAN facility and the medium range of operational temperature, the similar “hot-crucible” method with induction heating is chosen in the design due to its advantages mentioned above. During the preparation period of a melt droplet, the droplet is prevented by an Aerodynamic Levitation System (ALS) from falling out of the crucible. To design the heating system, the COMSOL code is applied to simulate the induction heating characteristics of a graphite crucible under different current and frequency of the work coil (inductor). Based on the simulation results, the induction heating system has been setup. A test of the heating system is also performed, and the

measured temperature has a good agreement with the predicted under the same frequency and current of the inductor, indicating a reasonable design of the heating system in the VULCAN facility.

## 2. Experimental Setup

Figure 1 shows a schematic of the experimental apparatus, which includes induction heating system, interaction zone, external trigger system, data acquisition system, inert gas levitation and protection system, and high-speed photography system.

Induction heating system is mainly composed of a furnace, an induction heater (host and controller), and an industrial chiller.

Figure 2 shows the structure of furnace, which includes a furnace shell, an insulated pipe, and a crucible. The furnace shell is stainless steel cylinder and its outer diameter, inner diameter, and height are 180 mm, 170 mm, and 135 mm, respectively. The crucible is supported by a tube, which can adjust the crucible to the specified position, and an observation window is placed at the top of the furnace for watching and photographing the heating state in the crucible. Argon is filled from the bottom of furnace at a flow rate range of  $1\sim10\times10^{-5}\text{ kg/m}^3$  to provide the levitation force and protective atmosphere.

The heating element is an induction coil, which is buried in MgO thermal insulation powders between furnace shell and insulated pipe. As shown in Figure 3, the spiral coil is made of 5 turns spiral copper pipe. The inside diameter, outside diameter, and height for the spiral coil are 66 mm, 82 mm, and 60 mm, respectively. The inner diameter and outer diameter of copper pipe are 6 mm and 8 mm.

The crucible has a double-layer structure that has two advantages:

- (i) The inner and outer crucible can be made of different materials. Materials with good induction heating effect can be adopted for the outer crucible, whereas materials that do not react with experimental materials can be selected for the inner crucible to ensure the intact droplet. In this work, both the inner crucible and the outer crucible are made of graphite.
- (ii) The inner crucible can be taken out freely for replacement, whereas the thermocouple can be fixed in the positioning hole of the outer crucible to measure the temperature of the crucible.

Figures 4 and 5 show the dimensions of the inner crucible and the outer crucible in the single-drop furnace.

The coil is power supplied by a medium-frequency power (GYM25AB). The nominal output electrical power and frequency are 25 kW and 47 kHz, respectively, determined by simulation and experiment. The current in the coil is adjustable for different heating temperature requirements.

A 5 HP industrial chiller is equipped to cool the induction heaters and the coils. The cooling capacity of the chiller is 13350 W, and the target outlet temperature can be set to specified value.

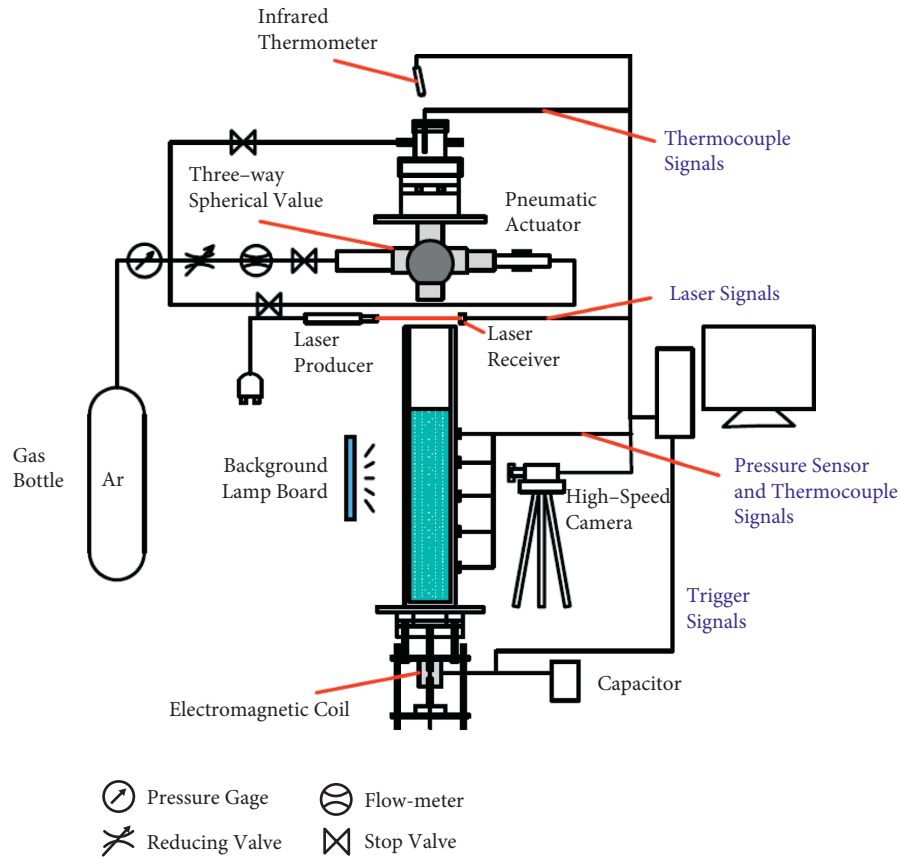


FIGURE 1: Schematic of test facility.

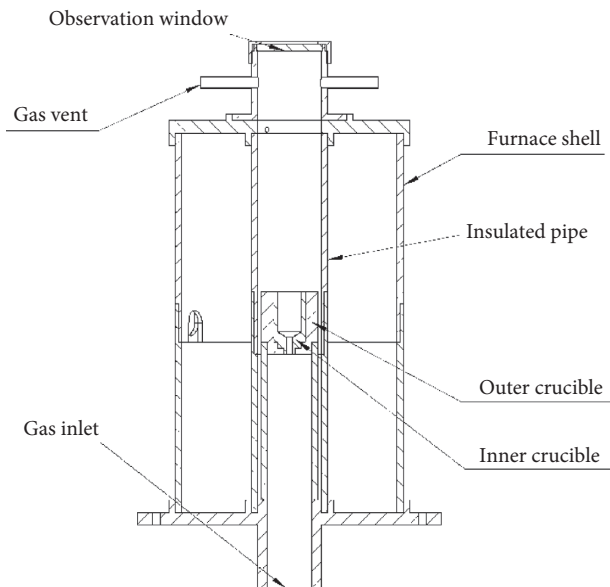


FIGURE 2: Schematic of the furnace for single droplet.

### 3. COMSOL Model of Simulation

**3.1. COMSOL Multiphysics.** The preparation of the melt is an important process of FCI experiment. In order to guide the design of crucible and coil, COMSOL Multiphysics® (referred as COMSOL) was used to simulate electromagnetic

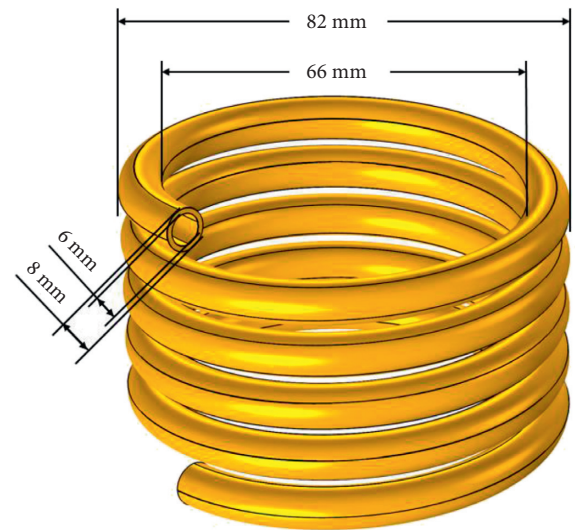


FIGURE 3: Schematic of the inductor (work coil).

induction and solid heat transfer phenomenon to obtain the melt condition under different operating parameters and provide a reference for experimental operation. COMSOL is an advanced numerical simulation software designed with finite element analysis method. It has the advantages of wide application range, easy operation, and multiphysical field coupling analysis [31].

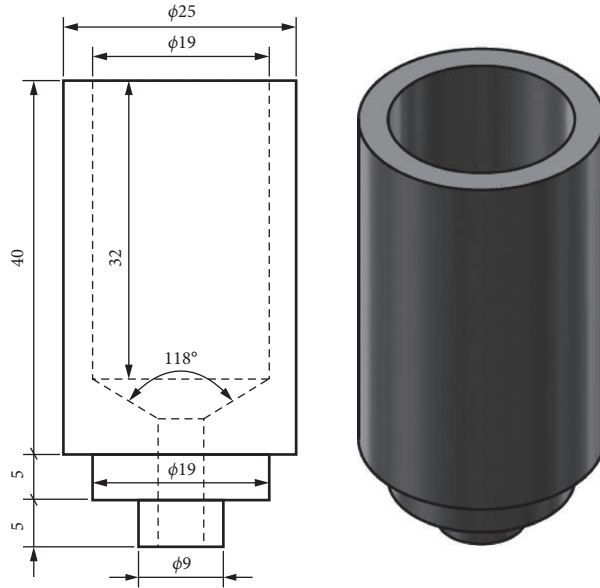


FIGURE 4: Dimensions ((a), unit: mm) and schematic (b) of the inner crucible.

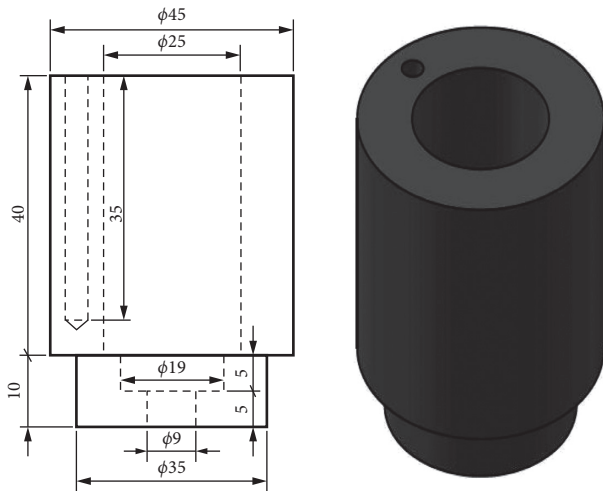


FIGURE 5: Dimensions ((a), unit: mm) and schematic (b) of the outer crucible.

**3.2. Geometric Model.** The geometric models and dimensions of inner and outer crucible are shown in Figures 4 and 5. The positioning hole of thermocouple in the outer crucible was ignored in this simulation.

For COMSOL, two methods can be used to build the coil area geometric model. One is to build the spiral coil structure directly, as shown in Figure 6(a). The other is to simplify the coil into a cylindrical structure with the setting of the coil parameters, which is only applicable for regular coils, as shown in Figure 6(b). The first method can be used to obtain the real current distribution in the coil wire and the real magnetic field distribution. The second method can only obtain the real magnetic field distribution, while the simulation speed is significant improved. In this article, we did not focus on the current distribution in the wire of the coil, and thus, the second method is selected for modeling.

**3.3. Mesh.** The numerical simulations were carried out on a block-structured mesh, which is obtained by rotation of the cross section. In addition, a mesh-sensitivity analysis was conducted by considering the meshes numbers that ranged from 8,104 to 785,993, under the coil current of 100 A and the frequency of 47 kHz. The average temperature and maximum temperature in the crucible were taken as verification criteria. Figure 7 shows the variation of the number of criteria with the number of grids. When the number of grids reaches 41,508, the differences of simulation results is small enough. Therefore, the grid with total number of 75,152 shown in Figure 8 were used for subsequent calculations, and the mesh quality is shown in Figure 9.

**3.4. Physical Model.** Magnetic insulation boundary where the magnetic field disappears is necessary to be defined in electromagnetic simulation calculation. In this work, the maximum boundary diameter of the coil is 82 mm. Therefore, the sphere boundary with a diameter of 200 mm is enough to define as magnetic insulation boundary. Solid coupling model was selected to describe the close contact of double-layered crucibles. Forced convection heat model was selected as the thermal boundary condition of the inner crucible cooling by argon.

According to the results from He and Xiao [32], the convective heat transfer coefficient was about 100 W/(m<sup>2</sup>·K). The outer boundary of the outer crucible applies natural convection, and the heat transfer coefficient is 35 W/(m<sup>2</sup>·K) [32]. The water loop inside copper tube the coil was set as isothermal boundary condition with a temperature of 30°C.

The physical properties of materials used in the model are shown in Table 1. The range of coil current is 20–500 A, and the range of frequency is 10–200 kHz in simulation.

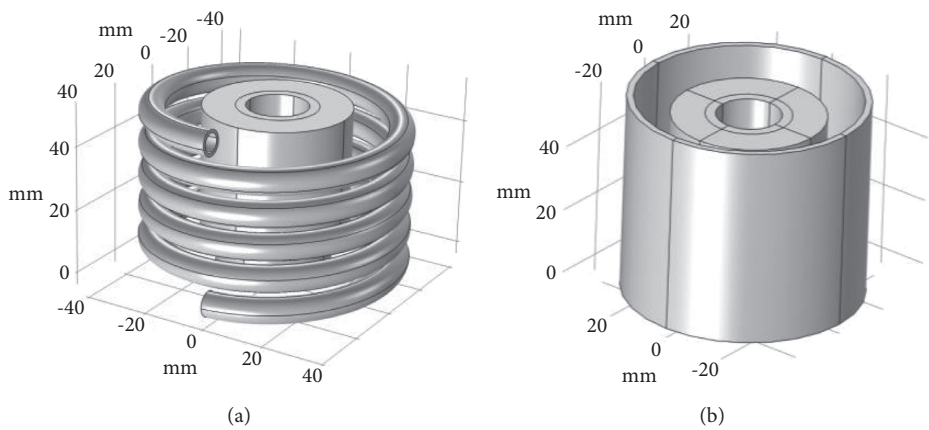


FIGURE 6: Two modeling methods in COMSOL.

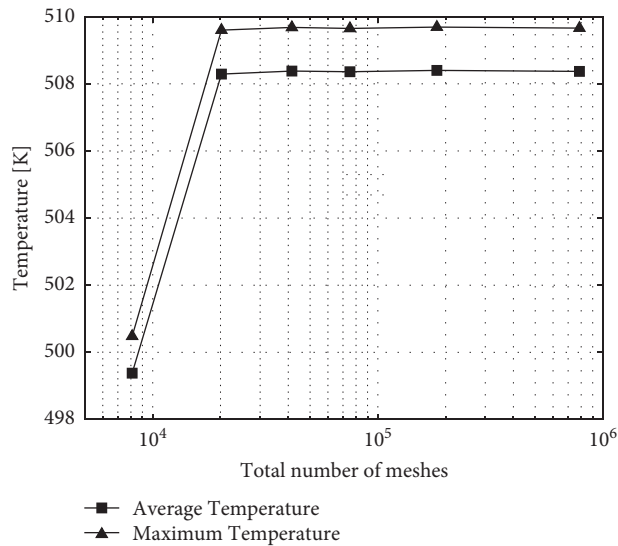


FIGURE 7: The average and the maximum temperature variations with total number of mesh.

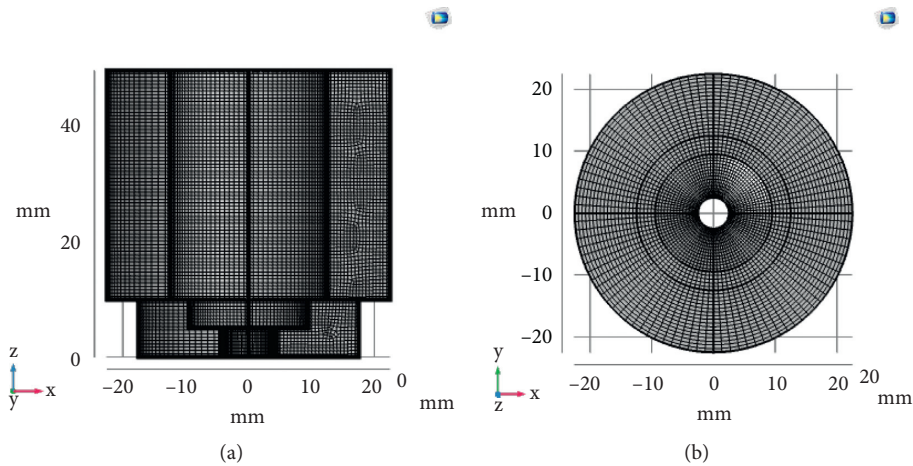


FIGURE 8: The view of mesh. (a) The cross section view of crucible. (b) The top view of crucible.



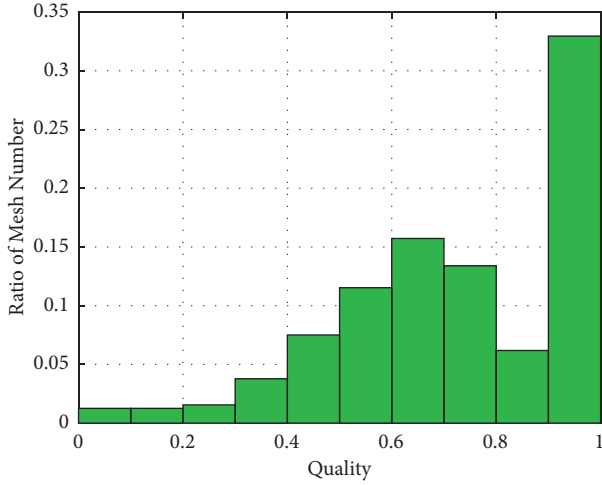


FIGURE 9: The quality of mesh (worse in left and better in right).

TABLE 1: The physical properties of materials.

Material	Argon	Graphite	Copper	Water
Relative permittivity	1	10 <sup>a</sup>	1	Default
Electrical conductivity (S/m)	0.01	1e5 <sup>b</sup>	5.88e7 <sup>d</sup>	5.5e-6 <sup>c</sup>
Relative permeability	1	1	1	Default
Specific heat capacity [J/(kg·K)]	Default	707.7 <sup>c</sup>	385.0 <sup>d</sup>	Default
Density [kg/m <sup>3</sup> ]	Default	Default	Default	Default
Thermal conductivity [W/(m·K)]	Default	24.0 <sup>c</sup>	385.0 <sup>d</sup>	Default

<sup>a</sup>Data from reference [33], <sup>b</sup>data from reference [34], <sup>c</sup>data from reference [35], and <sup>d</sup>data from reference [36].

## 4. Results and Discussion

**4.1. Skin Effect.** The skin effect of high-frequency electromagnetic induction has an important effect on the distribution of magnetic field. In order to study the skin effect, induction-heating simulation with different coil current frequencies was carried out.

The magnetic flux density distribution under the coil current of 100 A and frequency of frequency 10 kHz(a), 47 kHz(b), or 200 kHz(c) are shown in Figure 10. All of results show that the magnetic flux density is obviously concentrated on the outer surface of the crucible, and for the higher current frequency, the skin effect is more significant. The effects of frequencies on the magnetic flux density of cross section at the height of 25 mm are shown in Figure 11, and the skin depth (1/e) standard line is shown by the dashed line in this figure. It can be learnt that when the frequencies is 10 kHz or 20 kHz, the magnetic flux density distribution in the crucible is smoother, which means the thickness of the crucible wall does not reach the skin depth.

Focus on the distribution of flux density varies with depth at a certain frequency, taking the flux density distribution under the frequency of 200 kHz and the current of 100 A as an example. The exponential function is used for fitting, and the results are as follows:

$$\ln\left(\frac{B}{B_{\max}}\right) = -0.2519x - 0.0184, \quad (1)$$

where  $B$  is the magnetic flux density,  $B_{\max}$  is the maximum of the magnetic flux density,  $x$  is the depth from the surface of the crucible, and correlation coefficient is 0.9943.

The curve of skin depth with frequency is shown in Figure 12, which was obtained from Figure 10. The theoretical curve is calculated from the skin depth formula [37]:

$$\delta = \sqrt{\frac{2}{\mu\omega\sigma}}, \quad (2)$$

where  $\mu$  is the magnetic permeability in [H/m],  $\omega$  is the angular frequency in [rad/s],  $\sigma$  is the conductivity in [S/m], and  $\delta$  is the skin depth in [mm].

Under the frequency of 47 kHz, the theoretical value of skin depth is 7.34 mm, the simulated value is 8.15 mm, and the difference is 11%. Under the frequency of 100 kHz, the theoretical value of skin depth is 3.56 mm, the simulated value is 3.60 mm, and the difference is 1%. It can be seen from Figure 12 that the simulated calculation results are roughly consistent with the theoretical values, and the simulation deviation may be caused by the uneven distribution of the magnetic flux density on the Z coordinate since the length of the coil is finite and the shape of crucible is irregular.

Figure 13 shows the distribution of the current density at different frequency and same current of 100 A. Compared with Figures 10 and 13, it can be seen that the distribution of current density in the crucible is gentler than the distribution of magnetic flux density, which follows the skin depth of equation (1). Therefore, the skin depth of the current is deeper and the penetration ability is stronger, as shown in Figures 14 and 15.

The temperature distribution of the crucible cross section at the height of 25 mm under the coil current of 100 A and the frequency of 47 kHz is shown in the Figure 16. A high-temperature zone forms in the middle outboard part of the crucible. Conversely, a cold zone forms in the inner bottom part of the crucible. This temperature difference may be due to the skin effect of induced current, which caused the outboard Joule heat higher than inboard part, and the argon forced convection cooling inside the crucible. The maximum temperature difference between two zones mentioned above is about 1%.

The crucible is heated by the Joule heat of the eddy current, while the distribution of temperature in the crucible is flatter than the distribution of current. Because the thermal conductivity of graphite crucible is good, the temperature difference in the crucible is small, although the distribution of internal heat source caused by the skin effect of current is obviously uneven. Therefore, it is reasonable to measure the temperature at mounting position shown in Figure 5 as the crucible temperature.

**4.2. Effect of Inductor's Current and Frequency.** The magnitude and the frequency of the coil current are important factors of induction heating. As shown in Figures 17 and 18,

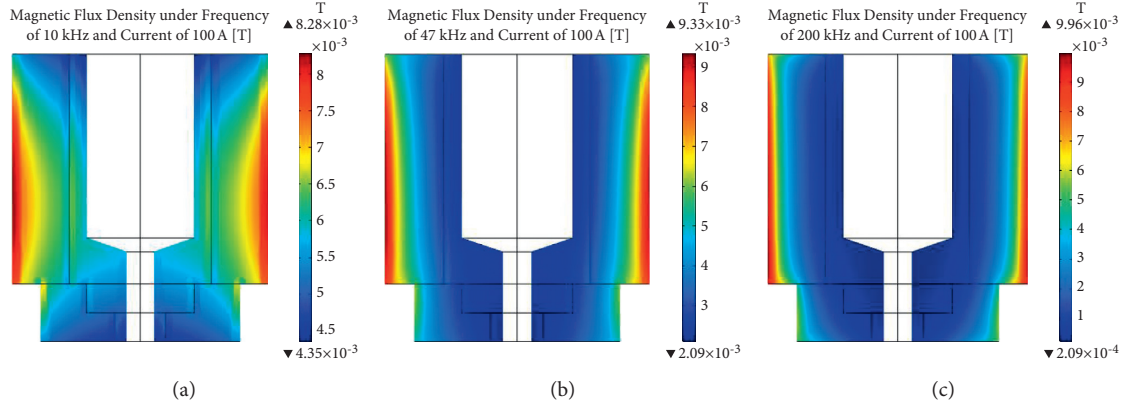


FIGURE 10: Distribution of magnetic flux density at different frequency and same current of 100 A.

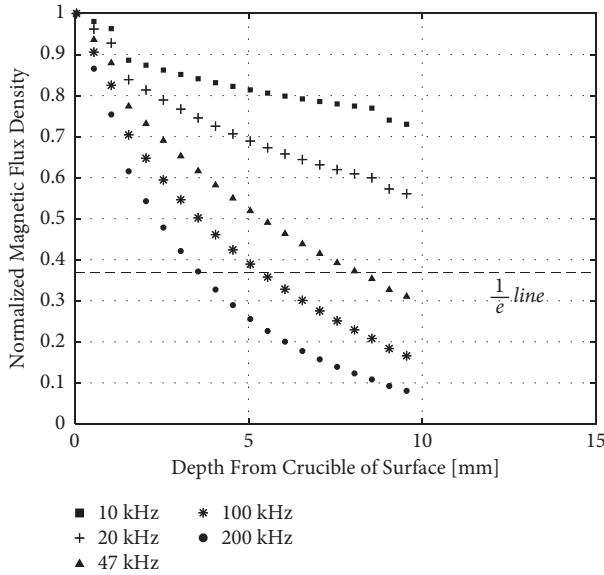


FIGURE 11: Magnetic flux density of cross section at the height of 25 mm under different frequencies.

when the coil current is maintained at 100 A, the average magnetic flux density and the average induced current density in the crucible increased with the increase in frequency; besides, the average magnetic flux density and the average induced current density increased more rapidly at low frequency. When the current frequency is 47 kHz, the average magnetic flux density has reached 98% of it at the frequency of 200 kHz and the average current density has reached 80% of it at the frequency of 200 kHz.

Figures 19 and 20 show the mean temperature and the distribution of temperature under different frequency, respectively. With the consideration of the skin depth in magnetic field, cost performance, and uniformity of temperature distribution, the calculated frequency of 50 kHz was selected for experiment bench design, and the actual manufactured frequency was 47 kHz. Figure 21 shows the average temperature of crucible under different coil currents and frequency. With the increase of coil current, the average

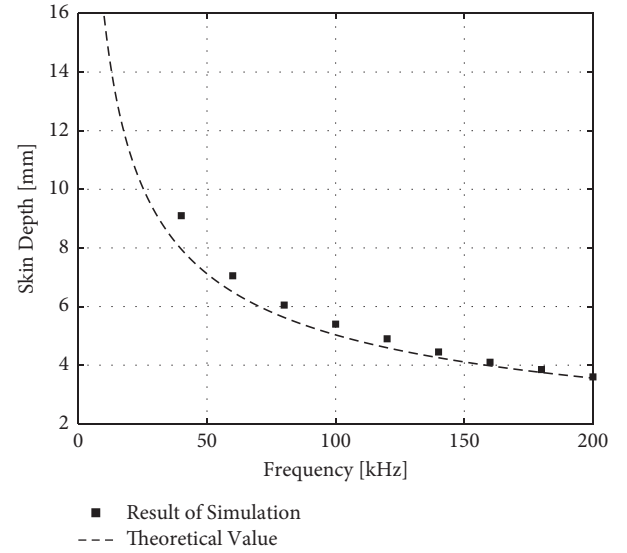


FIGURE 12: Skin depth variation with frequency.

temperature of the crucible increases exponentially. This correspondence could be expressed as follows:

$$\ln(T_{\text{mean}}) = 5.64 + 0.00702 * I(f = 47 \text{ kHz}), \quad (3)$$

where the correlation coefficient is 0.9928.

$$\ln(T_{\text{mean}}) = 5.55 + 0.00553 * I(f = 20 \text{ kHz}), \quad (4)$$

where the correlation coefficient is 0.9974,  $T_{\text{mean}}$  is the average temperature of the crucible,  $I$  is the magnitude of coil current, and  $f$  is the frequency of coil current. It should be noted that the melting model was not considered in the simulation calculation model, and the calculated temperature may reach more than the melting point of graphite.

As shown in Figure 22, the temperature inhomogeneity of the crucible increases as the coil current increases. The temperature inhomogeneity is about 4% and 10% under the coil current of 300 A and 500 A, respectively. When the current below 100 A, the temperature inhomogeneity can be almost ignored.

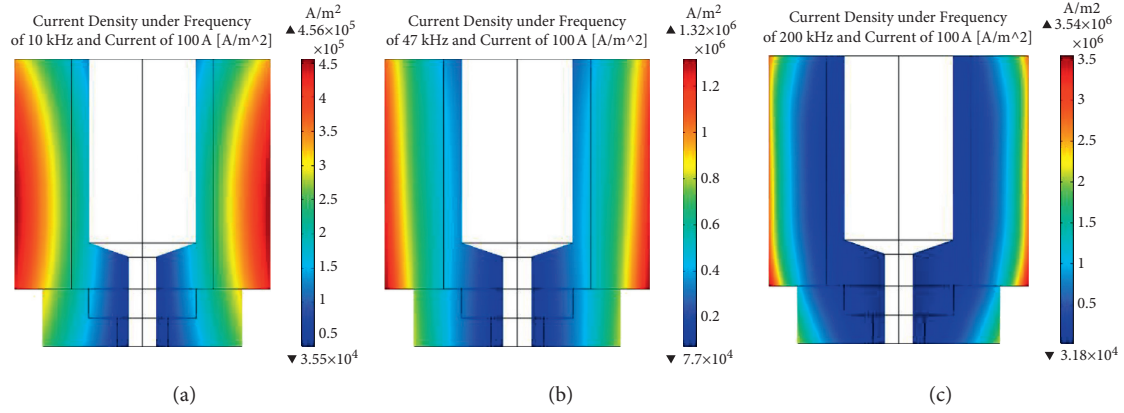


FIGURE 13: Distribution of current density at different frequency and the same current of 100 A.

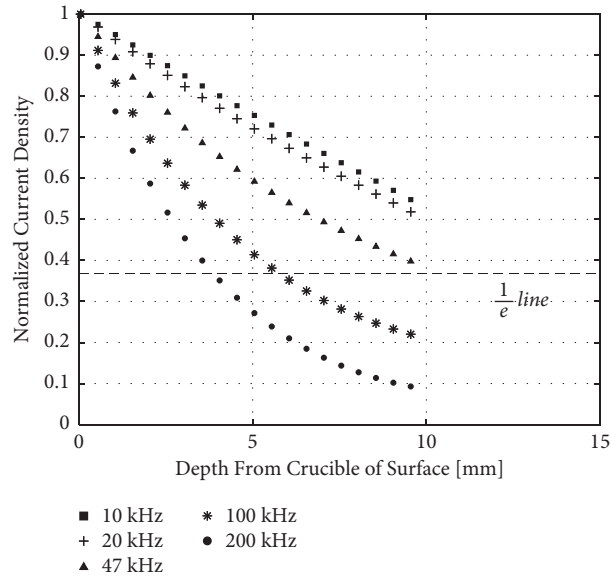


FIGURE 14: Current density of cross section at the height of 25 mm under different frequencies.

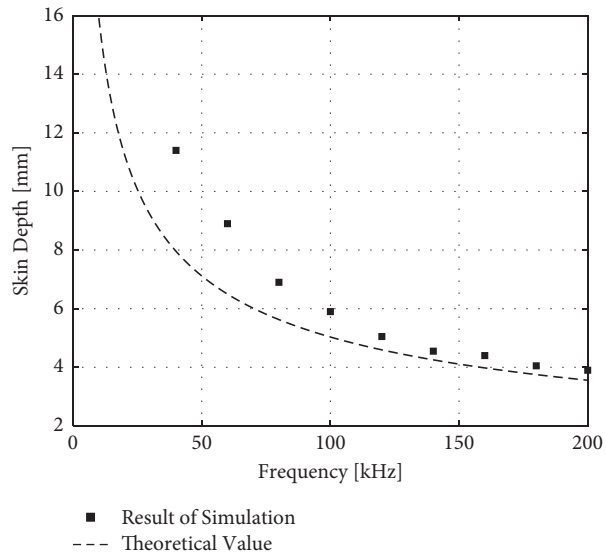


FIGURE 15: Skin depth variation with frequency.



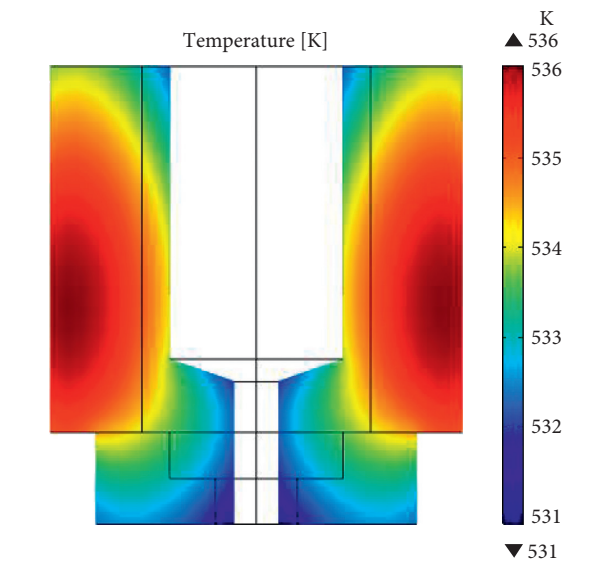


FIGURE 16: Cloud image of temperature distribution in the crucible’s cross section.

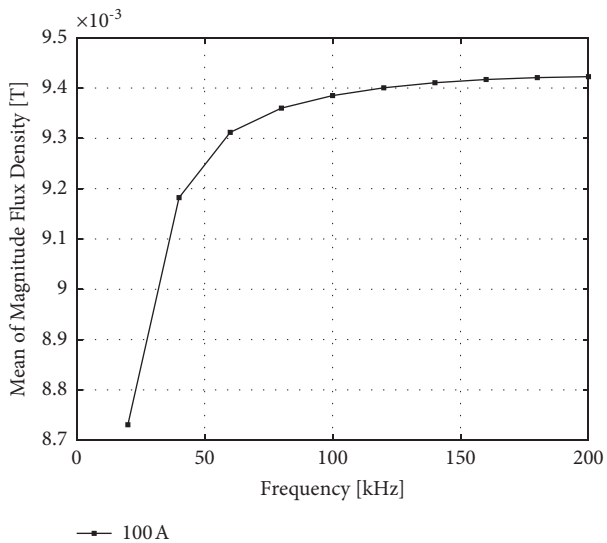


FIGURE 17: Mean of magnetic flux density varies with frequency.

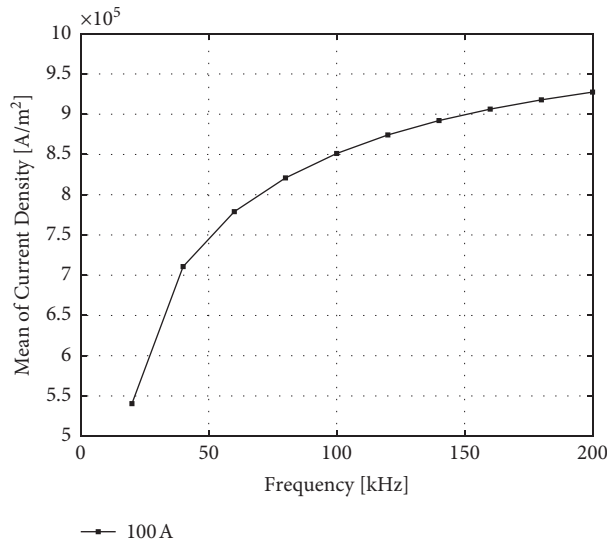


FIGURE 18: Mean current density variation with frequency.

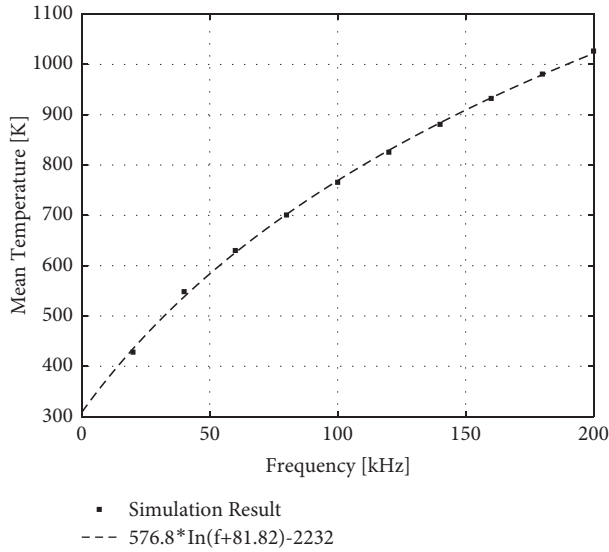


FIGURE 19: Mean temperature variation with frequency.

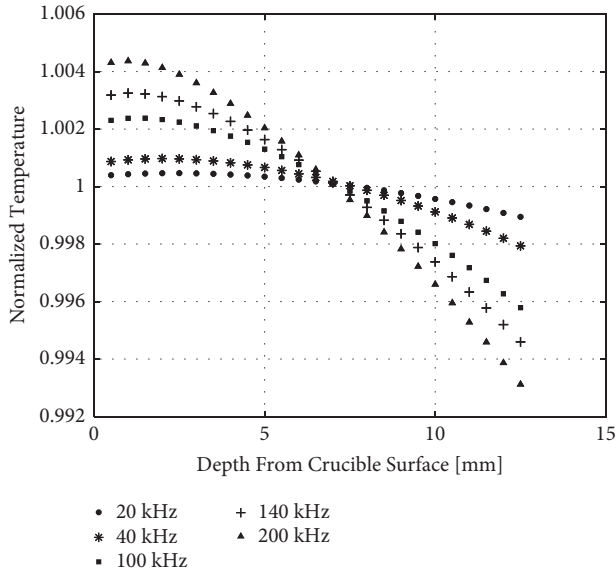


FIGURE 20: Distribution of temperature under different frequency.

The crucible can be heated to more than the heating requirement of 2500 K by the adjusted coil output current within 300 A under the frequency of 47 kHz, and the temperature difference in the crucible is less than 4% under this condition.

## 5. Testing of the Heating System

A test is conducted with the induction heating system whose current ranges from 40 A to 250 A under the frequency of 47 kHz, given the furnace and crucible as described in the preceding section. A C-type thermocouple and an infrared thermometer are used to measure the crucible's temperature below 1500 K and above 1500 K, respectively.

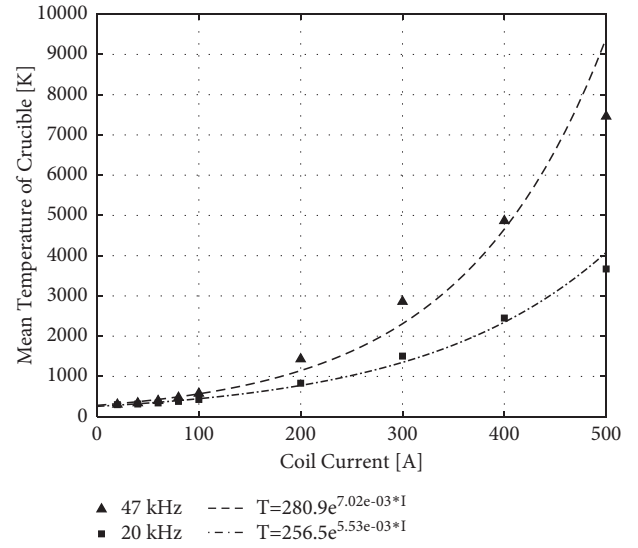


FIGURE 21: Average temperature of the crucible vs. inductor's current.

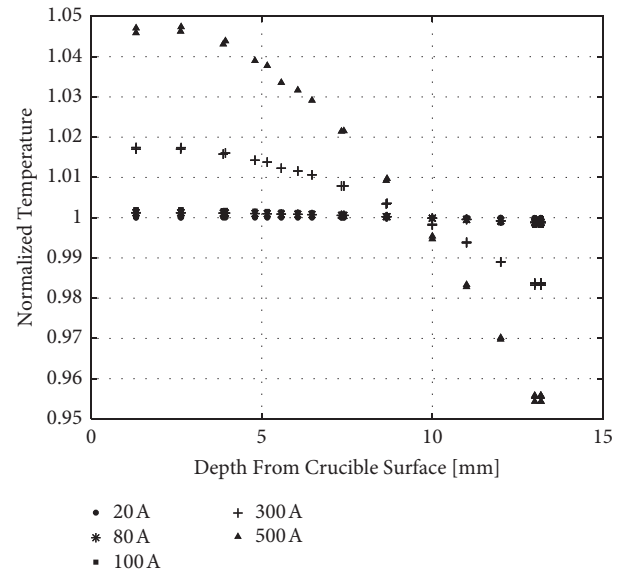


FIGURE 22: Normalized temperature profile along the cross section of the crucible at the height of 25 mm under different inductor's current and the same frequency.

TABLE 2: Comparison of measured and simulated temperatures.

Current of inductor (A)	Measured (K)	Simulated (K)	Absolute deviation (K)	Relative deviation
40.3	343.9	338.6	-5.3	-1.5%
59.8	402.1	395.5	-6.6	-1.6%
81.1	497.4	475.1	-22.3	-4.5%
99.7	612.7	577.4	-35.3	-5.8%
200.0	1509.8	1431.4	-78.4	-5.2%
251.3 <sup>a</sup>	2364.1 <sup>a</sup>	—	—	—

<sup>a</sup>The experiment of 300 A was not carried out because the predicted temperature under this condition is close to the melting point of graphite.

The crucible's temperatures measured in the test and predicted in the simulation are shown in Table 2. The maximum difference between the measured and predicted temperatures is 5.8%, which indicates the reasonable design of the induction heating system.

## 6. Conclusions

Motivated by the development of the test facility VULCAN to investigate melt-coolant interaction, the induction heating of a graphite crucible was simulated by the COMSOL code and studied, with the objective to design the heating system for the facility. Based on the simulation results and a verified test on the facility, the following conclusions can be drawn:

- (i) The skin effect of induction heating is reproduced by the COMSOL simulation, with the magnetic flux density concentrated on the outer surface of the crucible and decreasing exponentially with the depth from the outer surface.
- (ii) The heating power increases with the increase of the inductor's frequency and current. The average temperature of the crucible increases exponentially with the increase of the inductor's current. The temperature difference in the crucible is negligible, i.e., insensitive to the skin effect. Hence, it is reasonable to measure the temperature of the outer crucible as the average temperature of the crucible.
- (iii) In the verified test performed on the facility, the maximum difference between the measured and predicted temperatures of the crucible is 5.8%, indicating the capability of COMSOL for such simulation and the reasonable design of the heating system.

## Data Availability

The data used to support the findings of this study are included within the article.

## Conflicts of Interest

The authors declare that they have no conflicts of interest.

## Acknowledgments

The authors are grateful for the financial support of the Fundamental Research Funds for the National Key R&D Program of China (Grant no. 2018YFB1900100).

## References

- [1] L. Cizelj, B. Koncar, and M. Leskovic, "Vulnerability of a partially flooded PWR reactor cavity to a steam explosion," *Nuclear Engineering and Design*, vol. 236, no. 14, pp. 1617–1627, 2006.
- [2] G. Berthoud, "Vapor explosions," *Annual Review of Fluid Mechanics*, vol. 32, no. 1, 2000.
- [3] D. T. P. S. T. H. Lma, "Oecd programme serena (steam explosion resolution for nuclear applications) work programme and first results," *Work*, vol. 21, pp. 1–13, 2003.
- [4] OECD/NEA, "Agreement on the OECD/NEA SERENA Project – to address remaining issues on fuel-coolant interaction mechanisms and their effect on ex-vessel steam explosion energetics," 2008.
- [5] W. Klein-Heling, M. Sonnenkalb, D. Jacquemain, B. Clément, and I. Lindholm, "Conclusions on severe accident research priorities," *Annals of Nuclear Energy*, vol. 74, pp. 4–11, 2014.
- [6] S. J. Board and R. W. Hall, "Recent advances in understanding large scale vapor explosions," in *Proceedings of the Communication Safety and Nuclear Installation Meeting*, pp. 249–293, Sodium-Fuel Interact. Fast Reactor, Tokyo, Japan, September 1976.
- [7] R. Freud, R. Harari, and E. Sher, "Collapsing criteria for vapor film around solid spheres as a fundamental stage leading to vapor explosion," *Nuclear Engineering and Design*, vol. 239, no. 4, pp. 722–727, 2009.
- [8] J. W. Stevens and L. C. Witte, "Destabilization of vapor film boiling around spheres," *International Journal of Heat and Mass Transfer*, vol. 16, no. 3, pp. 669–670, 1973.
- [9] L. Manickam, S. Thakre, and W. Ma, "An experimental study on void generation around hot metal particle quenched into water pool," *International Topical Meeting on Nuclear Reactor Thermal Hydraulics*, vol. 32, 2015.
- [10] A. Inoue and S. G. Bankoff, "Destabilization of film boiling due to arrival of a pressure shock—part i: experimental," *Journal of Heat Transfer*, vol. 103, no. 3, 1981.
- [11] A. Sakurai, M. Shiotsu, and K. Hata, "Effects of system pressure on minimum film boiling temperature for various liquids," *Experimental Thermal and Fluid Science*, vol. 3, no. 4, pp. 450–457, 1990.
- [12] H. Kim, J. Buongiorno, L. W. Hu, T. J. McKrell, and G. L. Dewitt, "Experimental study on quenching of a small metal sphere in Nano-fluids," *ASME International Mechanical Engineering Congress & Exposition*, vol. 11, 2008.
- [13] T. Arai and M. Furuya, "Effect of hydrated salt additives on film boiling behavior at vapor film collapse," *Journal of Engineering for Gas Turbines & Power*, vol. 10, 2009.
- [14] P. K. Kanin, V. A. Ryazantsev, M. A. Lexin, A. R. Zabiroy, and V. V. Yagov, "Heat transfer enhancement at increasing water concentration in alcohol in the process of non-stationary film boiling," *Journal of Physics: Conference Series*, vol. 980, no. 1, Article ID 12029, 2018.
- [15] M. Pilch and C. A. Erdman, "Use of breakup time data and velocity history data to predict the maximum size of stable fragments for acceleration-induced breakup of a liquid drop," *International Journal of Multiphase Flow*, vol. 13, no. 6, pp. 741–757, 1987.
- [16] T. N. Dinh, V. A. Bui, and R. R. Nourgaliev, "Experimental and analytical studies of melt jet-coolant interactions: a synthesis," *Nuclear Engineering and Design*, vol. 189, no. 1, pp. 299–327, 1999.
- [17] K. H. Bang, J. M. Kim, and D. H. Kim, "Experimental study of melt jet breakup in water," *Journal of Nuclear Science and Technology*, vol. 40, no. 10, pp. 807–813, 2003.
- [18] B. W. Marshall, D. F. Beck, and M. Berman, "Mixing of isothermal and boiling molten-core jets with water: the initial conditions for energetic FCIs (fuel-coolant interactions)," in *Conference: International European Nuclear Society/American Nuclear Society Meeting on Thermal Reactor Safety*, Avignon, France, October 1988.

- [19] B. W. Spencer, J. D. Gabor, and J. C. Cassulo, "Effect of boiling regime on met stream breakup in water," in *Particulate Phenomena and Multiphase Transport*, T. N. Veziroglu, Ed., Hemisphere Publishing, London, UK, 1988.
- [20] D. Magallon and H. Hohmann, "High pressure corium melt quenching tests in FARO," *Nuclear Engineering and Design*, vol. 155, no. 1-2, pp. 253–270, 1995.
- [21] D. Magallon, I. Huhtiniemi, and H. Hohmann, "Lessons learnt from FARO/TERMOS corium melt quenching experiments," *Nuclear Engineering and Design*, vol. 189, no. 1-3, pp. 223–238, 1999.
- [22] D. Magallon and I. Huhtiniemi, "Corium melt quenching tests at low pressure and subcooled water in FARO," *Nuclear Engineering and Design*, vol. 204, no. 1-3, pp. 369–376, 2001.
- [23] A. Annunziato, A. Yerkess, and C. Addabbo, "FARO and KROTOS code simulation and analysis at JRC Ispra," *Nuclear Engineering and Design*, vol. 189, no. 1, pp. 359–378, 1999.
- [24] I. Huhtiniemi, D. Magallon, and H. Hohmann, "Results of recent KROTOS FCI tests: alumina versus corium melts," *Nuclear Engineering and Design*, vol. 189, no. 3, pp. 379–389, 1999.
- [25] J. H. Song, I. K. Park, Y. J. Chang, Y. S. Shin, J. H. Kim, and B. T. Min, "Experiments on the interactions of molten  $ZrO_2$  with water using TRIO facility," *Nuclear Engineering and Design*, vol. 213, no. 2, pp. 97–110, 2002.
- [26] T. A. Dullforce, D. J. Buchanan, and R. S. Peckover, "Self-triggering of small-scale fuel-coolant interactions: I. Experiments," *Journal of Physics D: Applied Physics*, vol. 9, no. 9, pp. 1295–1303, 2001.
- [27] L. S. Nelson and L. Buxton, *Steam Explosion Triggering Phenomena: Stainless Steel and Corium-E Simulants Studies with a Floodable Arc Melting Apparatus*, NUREG/CR-0112, Sandia National Lab, Albuquerque, NM, USA, 1978.
- [28] A. Karbojian, W. M. Ma, P. Kudinov, and T. N. Dinh, "A scoping study of debris bed formation in the DEFOR test facility," *Nuclear Engineering and Design*, vol. 239, no. 9, pp. 1653–1659, 2009.
- [29] P. Kudinov, A. Karbojian, C.-T. Tran, and W. Villanueva, "Agglomeration and size distribution of debris in DEFOR-A experiments with  $Bi_2O_3$ - $WO_3$  corium simulant melt," *Nuclear Engineering and Design*, vol. 263, pp. 284–295, 2013.
- [30] H. S. Park, R. C. Hansson, and B. R. Sehgal, "Fine fragmentation of molten droplet in highly subcooled water due to vapor explosion observed by x-ray radiography," *Experimental Thermal and Fluid Science*, vol. 29, no. 3, pp. 351–361, 2005.
- [31] "COMSOL," 2021, <http://cn.comsol.com/>.
- [32] C. He and F. Xiao, *Principles of Chemical Industry*, The Science Publishing Company, Singapore, 2007.
- [33] M. Hotta, M. Hayashi, M. T. Lanagan, D. K. Agrawal, and K. Nagata, "Complex permittivity of graphite, carbon black and coal powders in the ranges of X-band frequencies (8.2 to 12.4 GHz) and between 1 and 10 GHz," *ISIJ International*, vol. 51, no. 11, pp. 1766–1772, 2011.
- [34] P. N. Nirmalraj, T. Lutz, S. Kumar, G. S. Duesberg, and J. J. Boland, "Nanoscale mapping of electrical resistivity and connectivity in graphene strips and networks," *Nano Letters*, vol. 11, no. 1, pp. 16–22, 2011.
- [35] A. W. Blackwood, "Properties of pure metals, properties and selection: nonferrous alloys and special-purpose materials," in *ASM Handbook*, pp. 1099–1201, ASM International, Novelt, OH, USA, 1990.
- [36] R. L. David, *CRC Handbook of Chemistry and Physics*, CRC Press, Boca Raton, FL, USA, 80th edition, 1999.
- [37] H. A. Wheeler, "Formulas for the skin effect," *Proceedings of the IRE*, vol. 30, no. 9, pp. 412–424, 1942.